Croatian Society for Materials Protection

Metalurgija/Metallurgy

Vol. 66 No. 2 / 2027

Phase-State Control in As-Cast Cu–Al–Mn Shape Memory Alloys

Lovro Cigić [1,*], Aleš Nagode [1], Ivana Ivanić [2], Borut Kosec [1] and Blaž Karpe [1,*]

https://doi.org/10.64486/m.66.2.3

[1] University of Ljubljana, Faculty of Natural Sciences and Engineering (UL NTF), Aškerčeva cesta 12, 1000 Ljubljana, Slovenia; lovro.cigic@ntf.uni-lj.si, ales.nagode@ntf.uni-lj.si, borut.kosec@ntf.uni-lj.si, blaz.karpe@ntf.uni-lj.si

[2] University of Zagreb, Faculty of Metallurgy, Aleja narodnih heroja 3, 44000 Sisak, Croatia; iivanic@simet.hr

* Correspondence: blaz.karpe@ntf.uni-lj.si (B.K.); lovro.cigic@ntf.uni-lj.si (L.C.); Tel.: +386 1 2000 413 (B.K.); +386 1 2000 415 (L.C.)

Type of the Paper: Article

Received: June 5, 2026

Accepted: July 31, 2026

Abstract: Cu–Al–Mn shape memory alloys (SMAs) are attractive functional materials owing to their thermoelastic martensitic transformation, which enables the shape memory effect, superelasticity, and elastocaloric response. However, their practical application requires precise control of the transformation temperatures. In this study, the effect of Sn addition on the chemical homogeneity, microstructure, hardness, and transformation temperatures of as-cast Cu–Al–Mn–Sn alloys was investigated. CuAl9Mn9.5-based alloys with different Sn contents were fabricated by suction-assisted gravity casting, and their compositions were analyzed by energy-dispersive X-ray spectroscopy. Differential scanning calorimetry revealed that Sn addition systematically decreased the M_s, M_f, A_s, and A_f temperatures. A pronounced shift was already observed after adding 0.78 wt. % Sn, which reduced A_f from 102.4 to 23.4 °C. Further Sn additions shifted the transformation interval into the sub-zero temperature range, with A_f reaching −61.1 °C at 2.62 wt. % Sn. The transformation-temperature changes were accompanied by a transition from martensitic to austenitic room-temperature microstructure and increased hardness. These results demonstrate that Sn addition is an effective approach for tailoring the transformation temperature range of Cu–Al–Mn SMAs while maintaining casting consistency and chemical uniformity.

Keywords: Cu–Al–Mn shape memory alloy; Sn alloying; transformation temperatures; differential scanning calorimetry

1. Introduction

Cu–Al–Mn shape memory alloys (SMAs) have attracted sustained interest as functional materials because they exhibit a thermoelastic martensitic transformation that gives rise to the shape memory effect, superelasticity, and the elastocaloric effect [1–5]. This combination of functional properties, together with their relatively low material cost compared with many other SMAs, has made Cu–Al–Mn alloys particularly attractive. For practical applications, however, the functional response depends not only on the transformation mechanism itself but also on the temperatures at which it occurs. The characteristic transformation temperatures, M_s, M_f, A_s, and A_f define the temperatures at which the forward and reverse martensitic transformations begin and end. These temperatures

therefore determine the operational temperature window of the alloy and whether reversible transformation can be achieved under specific service conditions. This is particularly important for elastocaloric applications, where the alloy should be fully austenitic before mechanical loading, meaning that A_f must be below the intended operating temperature [6–8].

The transformation temperatures of Cu–Al–Mn alloys are strongly governed by phase stability in the parent β-based structure and are therefore highly sensitive to chemical composition [9]. Previous studies have shown that variations in Al and Mn content can systematically shift the characteristic transformation temperatures, confirming that composition control is an effective way to position the martensitic transformation within a desired temperature range [10]. In addition, thermomechanical treatments and processing history can further influence the transformation response, reinforcing the need to report composition–temperature relationships under clearly defined processing conditions [11].

For practical use, the functional response of SMAs is also affected by mechanical stability, cycling behavior, and microstructural state. Modeling and experimental studies on SMA structures and elastocaloric components have shown that loading mode, geometry, deformation conditions, and fatigue resistance are critical for stable operation [12–14]. In Cu-based SMAs, microstructure is particularly important because grain size and heat-treatment state can strongly affect functional durability and reliability [15–18]. Consequently, when evaluating the effect of alloying additions on transformation temperatures, chemical homogeneity and casting quality must also be considered.

Minor alloying additions offer an additional route for tuning the transformation behavior of ductile Cu–Al–Mn alloys. Among these additions, Sn is of particular interest because it has been reported to lower transformation temperatures in Cu–Al–Mn-based SMAs [19]. Previous work on as-cast Cu–Al–Mn alloys has also shown that microstructure and phase transformation behavior are closely related in this family of alloys [20]. Therefore, a systematic assessment of Sn-containing Cu–Al–Mn alloys in the as-cast state is needed to clarify how Sn addition affects chemical uniformity, density, microstructure, and transformation temperatures.

In the present study, as-cast Cu–Al–Mn–Sn shape memory alloys were prepared by adding various amounts of Sn to a CuAl9Mn9.5 base composition. The cast rods were evaluated in terms of chemical homogeneity, density, room-temperature microstructure, and transformation temperatures. The main objective was to determine whether Sn addition can reliably shift the martensitic transformation interval from elevated temperatures to lower, including sub-zero temperatures while maintaining sufficient chemical uniformity and casting consistency.

2. Materials and Methods

Cu–Al–Mn and Cu–Al–Mn–Sn alloys were prepared by SP-MSM208 arc melter, followed by suction-assisted gravity casting into a copper mold with a cavity diameter of 4 mm and a length of 45 mm. The resulting as-cast rods had a mass of approximately 9 g. Before melting, the chamber atmosphere was conditioned by repeated evacuation and argon backfilling cycles using high purity argon (Ar 5.0). A titanium getter was also melted before alloy preparation to further reduce residual oxygen in the chamber. The purity of all starting elements exceeded 99.7 %.

Alloy preparation was conducted in two stages. First, a Cu–Al–Mn master alloy was fabricated, after which it was remelted with varying Sn additions. This procedure enabled better control of the base Cu–Al–Mn chemistry before modification with Sn. The base composition was fixed at 9 wt. % Al and 9.5 wt. % Mn, with Cu as the balance. The Cu/Al ratio was selected to remain within the β-phase compositional window and to target martensitic transformation temperatures close to room temperature [3,19]. Sn-free Cu–Al–Mn reference alloy and several Cu–Al–Mn–Sn alloys with different Sn additions were prepared to isolate the effect of Sn while keeping the base Cu–Al–Mn composition unchanged.

Because arc melting can lead to preferential losses of volatile elements, especially Al and Mn, alloy compositions are reported both as nominal values calculated from charge masses and as post-melting values measured on the cast rods by EDXS. The arc melting setup, including the alloy charge and Ti getter, and the resulting as-cast rod are shown in Figure 1.

https://doi.org/10.64486/m.66.2.3

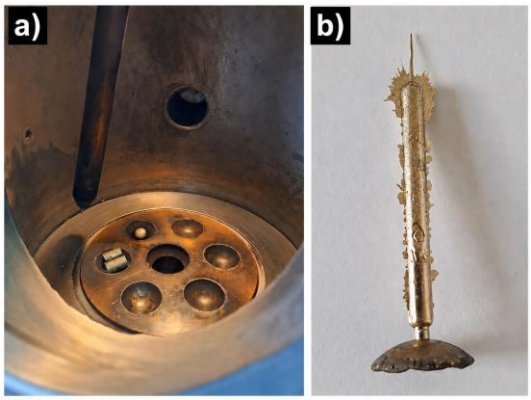

Figure 1. (a) Interior of the arc melting chamber with the alloy charge and Ti getter placed before melting; (b) as-cast rod produced by suction-assisted copper-mold casting.

Chemical composition was quantified by energy-dispersive X-ray spectroscopy (EDXS) using a Thermo Fisher Scientific Quattro S FEG-SEM equipped with an Ultim® Max detector in high-vacuum mode. Area-scan measurements were acquired at 20 kV and quantified using standardless analysis with matrix corrections. The reported compositions were normalized by excluding carbon and oxygen and are given for Cu, Al, Mn, and, where present, Sn. Chemical homogeneity was evaluated on longitudinal sections taken through the center of each rod, with measurements performed at three equally spaced positions along the 45 mm rod length, and on transverse mid-length cross-sections at the center and at three near-edge positions.

Microstructures were examined by optical microscopy (OM) using an Olympus DSX1000 3D digital microscope. Metallographic specimens were prepared using standard procedures for Cu-based alloys, including grinding and polishing, and were subsequently etched with a ferric chloride-based reagent consisting of 95 mL ethanol, 5 g $FeCl_3$, and 2 mL HCl.

Density was measured by Archimedes' principle using a KERN ABJ analytical balance with a resolution of 0.1 mg and a KERN ALS/PLS-A01 density kit. Distilled water was used as the immersion fluid, with a density of 997.928 kg m^{-3} at 21.3 °C. The density of each entire cast rod was measured three times, and the reported values represent the mean ± standard deviation of these repeated measurements. Density measurements were used as an additional indicator of casting consistency and to assess whether substantial porosity was introduced during rapid solidification. Vickers hardness was measured on polished transverse sections using a Wilson Instruments Tukon 2100B hardness tester. Measurements were performed using test forces of 9.81 N and 98.1 N, corresponding to HV1 and HV10, respectively, with a dwell time of 10 s. Each hardness value is reported as the mean ± standard deviation of three indentations.

Transformation temperatures were determined by differential scanning calorimetry (DSC) using a NETZSCH DSC 204 F1 Phoenix. DSC measurements were performed at heating and cooling rates of 10 K min^{-1} over the temperature range from −100 °C to 150 °C under an Ar purge at a flow rate of 20 mL min^{-1}, with liquid nitrogen used as the coolant. An empty aluminum crucible was used as the reference. The characteristic transformation temperatures, M_s, M_f, A_s, and A_f, were determined using the tangent method.

3. Results

3.1. Chemical homogeneity

Longitudinal and transverse analyses of the investigated rods revealed only minor compositional variations along the rod length and across the transverse cross-sections. The variations in the concentrations of the analyzed elements were generally within approximately ±0.5 wt. %, confirming the absence of significant chemical segregation in the cast rods. No discrete Sn-rich inclusions were observed within the spatial resolution of the EDXS measurements. Based on the observed compositional homogeneity, the bulk compositions reported in Table 1

https://doi.org/10.64486/m.66.2.3

were determined from large-area EDXS scans covering the largest possible area of the mid-length transverse cross-sections while excluding the surrounding background.

3.2. Chemical Composition and Transformation Temperatures

Table 1 summarizes the transformation temperatures obtained by DSC and the corresponding average compositions determined by EDXS. Figure 2 illustrates the variation of the characteristic transformation temperatures with Sn content.

Table 1. Transformation temperatures (Ms, Mf, As, Af) determined by DSC using the tangent method, and corresponding average compositions (EDXS) of CuAl9Mn9.5-based alloys with varying Sn contents.

Alloy composition (nominal)	**M_s °C**	**M_f °C**	**A_s °C**	**A_f °C**	**Al wt. %**	**Mn wt. %**	**Sn wt. %**	**Cu wt. %**
CuAl9Mn9.5	77.6	44.9	72.2	102.4	8.93	9.52	0.00	81.55
CuAl9Mn9.5Sn0.75	0.5	-16.4	6.6	23.4	9.21	9.49	0.78	80.52
CuAl9Mn9.5Sn1.5	-50.2	-66.3	-51.6	-34.4	8.78	9.66	1.41	80.15
CuAl9Mn9.5Sn2.5	-73.7	-86.6	-79.5	-61.1	8.82	9.57	2.62	78.99

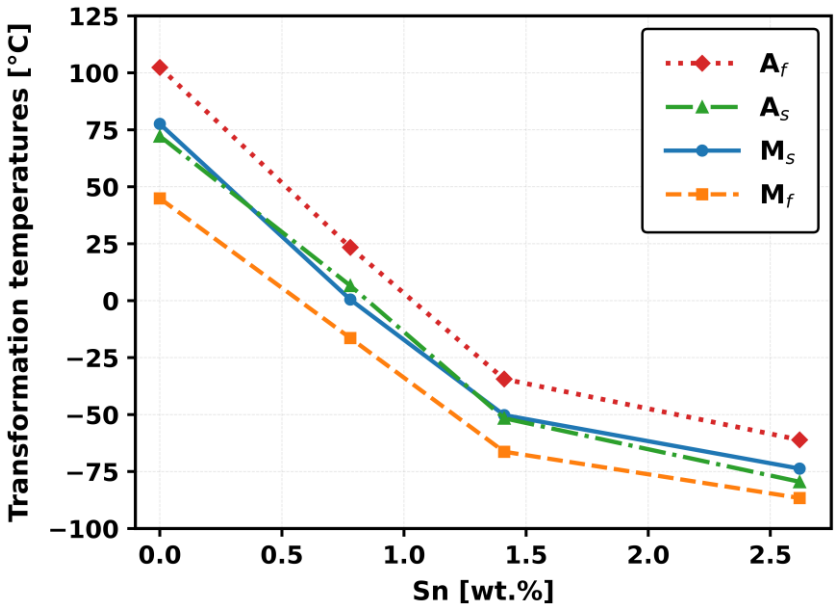

Figure 2. Effect of Sn content on the transformation temperatures (M_s, M_f, A_s, and A_f) of CuAl9Mn9.5-based alloys.

Increasing Sn content in the CuAl9Mn9.5 alloy systematically shifted both the forward transformation temperatures (M_s and M_f) and the reverse transformation temperatures (A_s and A_f) to lower temperatures. In the Sn-free reference alloy, A_f was 102.4 °C, indicating that the reverse transformation was completed well above room temperature. At 0.78 wt. % Sn, A_f decreased to 23.4 °C, while further increases in Sn content shifted the transformation interval into the sub-zero range. At 2.62 wt. % Sn, A_f decreased to −61.1 °C and M_f to −86.6 °C. These results demonstrate that Sn addition is an effective compositional strategy for lowering the transformation temperatures of Cu–Al–Mn–Sn shape memory alloys.

3.3. Microstructural Characteristics

Representative as-cast microstructures of the Sn-free reference alloy and the CuAl9Mn9.5Sn1.5 alloy were examined by optical microscopy to compare the room-temperature morphologies corresponding to different

https://doi.org/10.64486/m.66.2.3

phase states (Figure 3). The Sn-free CuAl9Mn9.5 alloy exhibited a microstructure characteristic of the martensitic state, consisting of dense colonies of martensitic plates/laths with a pronounced internally twinned substructure (Figure 3a). This morphology is consistent with the DSC results, which show that both A_s and A_f are above room temperature.

In contrast, the CuAl9Mn9.5Sn1.5 alloy showed an austenitic microstructure at room temperature (Figure 3b). The microstructure was dominated by equiaxed grains with orientation contrast and was clearly distinct from the plate/lath morphology observed in the Sn-free reference alloy (Figure 3a). This agrees with the DSC-derived transformation temperatures, where A_f is well below room temperature.

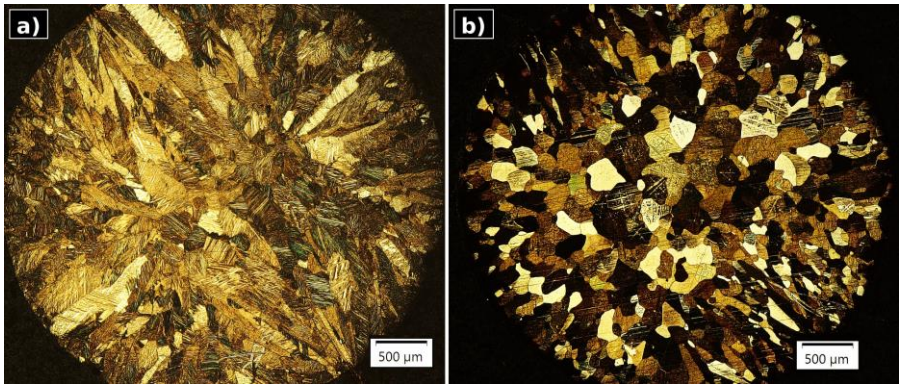

Figure 3. Microstructures of as-cast alloys: (a) CuAl9Mn9.5 and (b) CuAl9Mn9.5Sn1.5. The Sn-free alloy shows a martensitic plate/lath morphology, whereas the Sn-containing alloy shows an austenitic equiaxed-grain microstructure (OM).

3.4. Density and hardness

Table 2 summarizes the density and Vickers hardness of four as-cast CuAl9Mn9.5-based alloys with Sn contents ranging from 0 to 2.5 wt. %. The density of each entire cast rod was measured three times, and the corresponding mean values and standard deviations are reported in Table 2. To evaluate the density distribution along the rod length, each rod was subsequently sectioned into three approximately equal sections, and the density of each section was determined separately. The densities of the individual rod sections deviated from the corresponding whole-rod density by no more than 0.75 %. Furthermore, the whole-rod densities of the alloys with different Sn contents were comparable, ranging from 7.34 to 7.36 g/cm³, indicating that the addition of Sn had a negligible effect on the bulk density.

In contrast, the mean Vickers hardness increased systematically with increasing Sn content. The HV1 hardness increased from 180.5 for the Sn-free CuAl9Mn9.5 alloy to 207.2, 229.8, and 260.6 for the alloys containing 0.75, 1.5, and 2.5 wt. % Sn, respectively. A similar trend was observed for HV10, which increased from 170.0 to 191.3, 211.3, and 239.5, respectively. The higher HV1 hardness values compared with HV10 are likely related to the indentation size effect and the limited sampling volume of smaller indents, which makes the measurements more sensitive to local microstructural heterogeneities in the as-cast alloys. This systematic hardening accompanies the composition-dependent shifts in transformation behavior reported in Section 3.2 and the corresponding changes in microstructure at room temperature shown in Figure 3.

Table 2. Density and Vickers hardness of as-cast CuAl9Mn9.5-based alloys with increasing Sn content

Alloy (nominal)	ϱ / g/cm³	HV1	HV10
CuAl9Mn9.5	7.3613 ± 0.031	180.5 ± 4.2	170.0 ± 3.1
CuAl9Mn9.5Sn0.75	7.3594 ± 0.022	207.2 ± 3.8	191.3 ± 3.0
CuAl9Mn9.5Sn1.5	7.3551 ± 0.026	229.8 ± 4.7	211.3 ± 3.9
CuAl9Mn9.5Sn2.5	7.3438 ± 0.015	260.6 ± 5.2	239.5 ± 4.3

https://doi.org/10.64486/m.66.2.3

Note*: Whole-rod density values are reported as the mean ± standard deviation of three repeated measurements performed using Archimedes' method at 21.3 °C. HV1 and HV10 values are reported as the mean ± standard deviation of three indentations.*

4. Discussion

EDXS analyses along the rod axis and across representative cross sections indicated good chemical uniformity of the cast rods. The observed axial and radial variations were small compared with the systematic differences in Sn content between the investigated alloys. This is particularly important because the transformation temperatures of Cu–Al–Mn alloys are highly sensitive to relatively small variations in chemical composition [10,19]. Therefore, the pronounced composition-dependent shifts in transformation temperatures can reasonably be attributed primarily to the intentional Sn additions rather than to macroscopic chemical segregation. Furthermore, no discrete Sn-rich phases were detected in any Sn-containing alloy within the spatial resolution of the EDXS measurements. This suggests a relatively uniform Sn distribution at the examined scale; however, the precise solubility state of Sn cannot be confirmed without complementary phase analysis.

The whole-rod densities remained essentially unchanged over the investigated Sn range, varying only from 7.3613 to 7.3438 g/cm^3. This difference corresponds to approximately 0.24 % and is comparable to the experimental scatter, indicating that Sn addition up to 2.5 wt. % had no clearly measurable effect on the bulk density. The limited density variation along the rods further suggests comparable casting consistency among the investigated alloys, although density measurements alone cannot exclude fine scale microporosity. In contrast, the Vickers hardness increased systematically with increasing Sn content. HV1 increased from 180.5 to 260.6, corresponding to an increase of approximately 44 %, while HV10 increased from 170.0 to 239.5, corresponding to an increase of approximately 41 %. Previous studies have similarly shown that alloying additions can substantially affect the hardness of Cu–Al–Mn-based alloys and that hardness is sensitive to the structural and ordering state of the β-based phase [21,22]. The observed hardening may therefore reflect a combination of compositional solid solution strengthening associated with Sn addition and changes in the structural state of the alloys; however, the individual contributions cannot be distinguished from the present hardness measurements alone.

The DSC results show that Sn is an effective alloying element for lowering the transformation temperatures in the Cu–Al–Mn alloy system. Both the forward transformation temperatures, M_s and M_f, and the reverse transformation temperatures, A_s and A_f, decreased systematically with increasing Sn content. The strong sensitivity of the transformation temperatures to minor Sn additions is evident from the change observed after adding only 0.78 wt. % Sn, which reduced A_f and M_f by 79.0 and 61.3 °C, respectively, compared with the Sn-free alloy. Further increases in Sn content progressively shifted the transformation range into the subzero region, with A_f reaching −61.1 °C and M_f −86.6 °C at 2.62 wt. % Sn. The transformation intervals also became narrower after Sn addition. These results indicate that Sn not only shifts the transformation temperatures but also modifies the temperature range over which the transformation proceeds. The observed trend is consistent with previous reports showing that alloying additions and relatively small compositional changes can strongly affect the transformation behavior of ductile Cu–Al–Mn alloys [10,19]. The systematic decrease in all four characteristic temperatures suggests that Sn stabilizes the parent austenitic phase relative to martensite over a wider temperature range. This is relevant for applications requiring an austenitic initial state before stress-induced transformation, including elastocaloric operation [1,2,6–8].

The microstructural observations are consistent with the DSC-derived transformation temperatures. The Sn-free CuAl9Mn9.5 alloy exhibited a martensitic plate/lath morphology at room temperature, whereas CuAl9Mn9.5Sn1.5 showed an austenitic, equiaxed-grain morphology. For the Sn-free alloy, both A_s and A_f were above room temperature, which is consistent with the persistence of thermally induced martensite under ambient conditions. In contrast, the A_f temperature of the CuAl9Mn9.5Sn1.5 alloy was −34.4 °C, supporting the presence of the parent austenitic phase at room temperature. A similar relationship between the transformation-temperature range and the room-temperature microstructure has been reported for as-cast Cu-rich Cu–Al–Mn alloys [20]. This contrast supports the conclusion that sufficient Sn addition changes the room-temperature phase state of the CuAl9Mn9.5-based alloy by lowering the transformation temperatures. However, because optical microscopy

https://doi.org/10.64486/m.66.2.3

provides morphological rather than crystallographic phase identification, complementary X-ray diffraction or EBSD analysis would be required to confirm the phase constitution directly.

5. Conclusions

As-cast Cu–Al–Mn–Sn shape memory alloys with varying Sn contents were successfully prepared from a CuAl9Mn9.5 base composition by arc melting followed by suction-assisted copper-mold casting. EDXS and density measurements indicated good chemical uniformity and consistent casting quality, with no evidence of substantial macroscopic porosity. Vickers hardness increased with increasing Sn content, showing that Sn addition also influenced the mechanical response of the as-cast alloys.

DSC measurements showed that Sn addition effectively lowered the transformation temperatures in the CuAl9Mn9.5-based alloy system. Increasing Sn content shifted both the forward and reverse transformation temperatures from above room temperature toward lower, including the subzero range at higher Sn contents.

Microstructural observations supported the DSC results. The Sn-free alloy exhibited a martensitic plate/lath morphology, whereas the CuAl9Mn9.5Sn1.5 alloy showed an austenitic equiaxed-grain microstructure.

Overall, Sn addition provides an effective compositional route for tailoring as-cast CuAl9Mn9.5-based shape memory alloys toward lower transformation temperatures. Further work should examine intermediate Sn contents and the practical limits of Sn addition without compromising alloy processability. Sn-containing and Sn-free alloys should also be directly compared in terms of transformation hysteresis, transformation and recoverable strains, cycling stability, and elastocaloric performance under comparable thermomechanical conditions.

6. Acknowledgements

The authors acknowledge financial support from the Slovenian Research and Innovation Agency (ARIS) under project No. 30-ARIS.N2-0375, Advanced Elastocaloric Regenerators. The data generated and analyzed during this study are available from the corresponding author upon reasonable request. The authors declare that ChatGPT was used exclusively as a generative AI tool to assist with language editing, text-structure refinement, and formatting of selected manuscript sections. The authors reviewed and edited all AI-assisted content and take full responsibility for the content of the publication.

References

[1] S. Qian, Y. Geng, Y. Wang, T. E. Pillsbury, Y. Hada, Y. Yamaguchi, *et al*., "Elastocaloric effect in CuAlZn and CuAlMn shape memory alloys under compression," *Philosophical Transactions of the Royal Society A: Mathematical, Physical and Engineering Sciences*, vol. 374, no. 2074, Art. no. 20150309, 2016, https://doi.org/10.1098/rsta.2015.0309

[2] Y. Wu, E. Ertekin, and H. Sehitoglu, "Elastocaloric cooling capacity of shape memory alloys—Role of deformation temperatures, mechanical cycling, stress hysteresis and inhomogeneity of transformation," *Acta Materialia*, vol. 135, pp. 158–176, 2017, https://doi.org/10.1016/j.actamat.2017.06.012

[3] M. O. Prado, P. M. Decorte, and F. Lovey, "Martensitic transformation in Cu–Mn–Al alloys," *Scripta Metallurgica et Materialia*, vol. 33, no. 6, pp. 877–883, 1995, https://doi.org/10.1016/0956-716X(95)00292-4

[4] Y. Sutou, T. Omori, R. Kainuma, and K. Ishida, "Ductile Cu–Al–Mn based shape memory alloys: General properties and applications," *Materials Science and Technology*, vol. 24, no. 8, pp. 896–901, 2008, https://doi.org/10.1179/174328408X302567

[5] B. Kosec, B. Karpe, A. Nagode, M. Bizjak, L. Vrsalović, D. Ćubela, M. Gojić, I. Ivanić, and S. Kožuh, "Thermal properties of copper base shape memory alloy," in *Proceedings of the 14th Scientific-Research Symposium with International Participation, Metallic and Nonmetallic Materials: Production–Properties–Application*, Zenica, Bosnia and Herzegovina, 2023, pp. 133–138.

https://doi.org/10.64486/m.66.2.3

[6] S. Qian, Y. Geng, Y. Wang, J. Ling, Y. Hwang, R. Radermacher, I. Takeuchi, and J. Cui, "A review of elastocaloric cooling: Materials, cycles and system integrations," *International Journal of Refrigeration*, vol. 64, pp. 1–19, 2016, https://doi.org/10.1016/j.ijrefrig.2015.12.001

[7] Ž. Ahčin and J. Tušek, "Parametric analysis of fatigue-resistant elastocaloric regenerators: Tensile vs. compressive loading," *Applied Thermal Engineering*, vol. 231, Art. no. 120996, 2023, https://doi.org/10.1016/j.applthermaleng.2023.120996

[8] J. Tušek, K. Engelbrecht, R. Millán-Solsona, L. Mañosa, E. Vives, L. P. Mikkelsen, and N. Pryds, "The elastocaloric effect: A way to cool efficiently," *Advanced Energy Materials*, vol. 5, no. 13, Art. no. 1500361, 2015, https://doi.org/10.1002/aenm.201500361

[9] E. Yüzüak and G. Durak Yüzüak, "Introducing the chemical potential of Cu–Mn–Al alloys for structural, electrical and thermal properties," *Bulletin of Materials Science*, vol. 47, Art. no. 108, 2024, https://doi.org/10.1007/s12034-024-03216-1

[10] C. A. Canbay, Z. Karagoz, and F. Yakuphanoglu, "Controlling of transformation temperatures of Cu–Al–Mn shape memory alloys by chemical composition," *Acta Physica Polonica A*, vol. 125, no. 5, pp. 1163–1166, 2014, https://doi.org/10.12693/APhysPolA.125.1163

[11] D. Milosavljevic, N. Lecis, and S. Cinquemani, "Influence of thermomechanical treatments and chemical composition on the phase transformation of Cu–Al–Mn shape memory alloy thin sheets," *Applied Sciences*, vol. 14, no. 22, Art. no. 10406, 2024, https://doi.org/10.3390/app142210406

[12] L. Porenta, M. Lavrenčič, J. Dujc, M. Brojan, J. Tušek, and B. Brank, "Modeling large deformations of thin-walled SMA structures by shell finite elements," *Communications in Nonlinear Science and Numerical Simulation*, vol. 101, Art. no. 105897, 2021, https://doi.org/10.1016/j.cnsns.2021.105897

[13] L. Porenta, P. Kabirifar, A. Žerovnik, M. Čebron, B. Žužek, M. Dolenec, M. Brojan, and J. Tušek, "Thin-walled Ni-Ti tubes under compression: Ideal candidates for efficient and fatigue-resistant elastocaloric cooling," *Applied Materials Today*, vol. 20, Art. no. 100712, 2020, https://doi.org/10.1016/j.apmt.2020.100712

[14] Ž. Ahčin, S. Dall'Olio, A. Žerovnik, U. Ž. Baškovič, L. Porenta, P. Kabirifar, *et al.*, "High-performance cooling and heat pumping based on fatigue-resistant elastocaloric effect in compression," *Joule*, vol. 6, no. 10, pp. 2338–2357, 2022, https://doi.org/10.1016/j.joule.2022.08.011

[15] I. Ivanić, M. Gojić, S. Kožuh, and B. Kosec, "Microstructural analysis of CuAlNiMn shape-memory alloy before and after the tensile testing," *Materiali in tehnologije*, vol. 48, no. 5, pp. 713–718, 2014. [Online]. Available: http://mit.imt.si/izvodi/mit145/ivanic.pdf

[16] S. Yang, M. Chi, J. Zhang, Y. Lu, Y. Huang, C. Wang, and X. Liu, "Abnormal grain growth in annealing cast Cu–Al–Mn–V alloys and their superelasticity," *Smart Materials and Structures*, vol. 28, no. 5, Art. no. 055015, 2019, https://doi.org/10.1088/1361-665X/ab0b73

[17] T. Omori, T. Kusama, S. Kawata, I. Ohnuma, Y. Sutou, Y. Araki, *et al.*, "Abnormal grain growth induced by cyclic heat treatment," *Science*, vol. 341, no. 6153, pp. 1500–1502, 2013, https://doi.org/10.1126/science.1238017

[18] L. Vrsalović, I. Ivanić, S. Kožuh, B. Kosec, M. Bizjak, J. Kovač, U. Gabor, and M. Gojić, "Influence of heat treatment on the corrosion properties of CuAlMn shape memory alloys," *Corrosion Reviews*, vol. 37, no. 6, pp. 579–589, 2019, https://doi.org/10.1515/corrrev-2019-0034

[19] Y. Sutou, R. Kainuma, and K. Ishida, "Effect of alloying elements on the shape memory properties of ductile Cu–Al–Mn alloys," *Materials Science and Engineering: A*, vols. 273–275, pp. 375–379, 1999, https://doi.org/10.1016/S0921-5093(99)00301-9

https://doi.org/10.64486/m.66.2.3

[20] T. Holjevac-Grgurić, D. Manasijević, S. Kožuh, I. Ivanić, Lj. Balanović, I. Anžel, B. Kosec, M. Bizjak, M. Knežević, and M. Gojić, "Phase transformation and microstructure study of the as-cast Cu-rich Cu–Al–Mn ternary alloys," *Journal of Mining and Metallurgy, Section B: Metallurgy*, vol. 53, no. 3, pp. 413–422, 2017, https://doi.org/10.2298/JMMB170809039H

[21] R. Dasgupta, A. K. Jain, P. Kumar, S. Hussain, and A. Pandey, "Role of alloying additions on the properties of Cu–Al–Mn shape memory alloys," *Journal of Alloys and Compounds*, vol. 620, pp. 60–66, 2015, https://doi.org/10.1016/j.jallcom.2014.09.047

[22] M. O. Prado and A. Tolley, "Hardness of Cu–Mn–Al alloys as a function of the annealing temperature in the β phase," *Materials Science and Engineering: A*, vols. 273–275, pp. 590–594, 1999, https://doi.org/10.1016/S0921-5093(99)00435-9

https://doi.org/10.64486/m.66.2.3